# Formation and stabilization of $C_6^-$ by radiative electron attachment

Vijayanand Chandrasekaran, Aneesh Prabhakaran, Bhim Kafle, Hilel Rubinstein, Oded Heber, Michael Rappaport, Yoni Toker, and Daniel Zajfman

Citation: The Journal of Chemical Physics **146**, 094302 (2017); doi: 10.1063/1.4977059
View online: http://dx.doi.org/10.1063/1.4977059
View Table of Contents: http://aip.scitation.org/toc/jcp/146/9
Published by the American Institute of Physics

# Formation and stabilization of $C_6^-$ by radiative electron attachment

Vijayanand Chandrasekaran,[a] Aneesh Prabhakaran, Bhim Kafle, Hilel Rubinstein, Oded Heber, Michael Rappaport, Yoni Toker, and Daniel Zajfman
*Department of Particle Physics and Astrophysics, Weizmann Institute of Science, Rehovot 76100, Israel*

(Received 9 October 2016; accepted 9 February 2017; published online 2 March 2017)

Radiative electron attachment (REA) plays an important role in forming molecular anions in various astrophysical environments. In this work, we determined the rate coefficient for the formation of $C_6^-$ by REA based on a detailed balance approach. $C_6^-$ ions are stored in an electrostatic ion beam trap and are photoexcited above their adiabatic detachment energy (4.18 eV). Due to fast internal conversion and intramolecular vibrational redistribution, photoexcitation leads to the formation of temporary negative ions (TNIs), the same as those one formed by the electron attachment. Absolute vibrational autodetachment and recurrent (or Poincaré) fluorescence (RF) rate coefficients have already been reported [V. Chandrasekaran *et al.*, J. Phys. Chem. Lett. **5**, 4078 (2014)]. Knowing the branching ratios of the various competing rate coefficients is decisive to the understanding of the formation probability of anions via REA. The radiative stabilization rate of $C_6^-$, shown to be dominated by RF, was determined to be $5 \times 10^4$ s$^{-1}$ at the electron detachment energy, i.e., at least a factor of 100 faster than the stabilization by infrared transitions. The RF is found to very effectively stabilize the TNI formed by electron attachment. Using detailed balance to link the measured delayed detachment rate to the rate of electron attachment, we estimate the REA rate leading to the formation of $C_6^-$ to be $3 \times 10^{-7}$ cm$^3$ s$^{-1}$ at 300 K in agreement with theory ($1.7 \times 10^{-7}$ cm$^3$ s$^{-1}$ [R. Terzieva and E. Herbst, Int. J. Mass Spectrom. **201**, 135 (2000)]). Such a high rate for REA to $C_6$ indicates that REA may play a prominent role in the formation of anions in the interstellar medium. *Published by AIP Publishing.* [http://dx.doi.org/10.1063/1.4977059]

## I. INTRODUCTION

Using ground-based radio astronomy, several interstellar anions have been detected.[1–4] Most of these anions have been thought to be formed by radiative electron attachment (REA). Herbst has performed statistical calculations based on the phase space theory (PST) for the formation of molecular anions by REA.[5] Until now, most of the rate coefficients for REA have come from PST[5–8] and from quantum chemical calculations.[9,10] Unfortunately, to our knowledge, there were very little experimental data on the rate coefficients for REA processes in stable molecules,[11–13] and none for radicals. Rate coefficients obtained from PST have been included in chemical models to model various interstar environments.[14–18] For exact modeling of the chemical environments of various astronomical sources, rate coefficients for the formation of various species are need to be accurately known.

In REA, low energy electrons interact with molecules such as $C_6$ thereby forming an electron-molecule complex that can autodetach back to neutral $C_6$ and a free electron or it can form a temporary negative ion (TNI) in the ground electronic state with energy equal to the sum of kinetic energy of the incoming electron, initial internal energy of $C_6$, and the electron affinity of $C_6$. The TNI can autodetach back to a free electron and neutral $C_6$ or it can emit a photon that stabilizes the anion against autodetachment. The mechanism has been schematically represented in Fig. 1.

When $C_6^-$ is photoexcited by two-photon excitation, internal conversion (IC) is followed by intramolecular vibrational redistribution (IVR) in a time scale of 620 fs.[19,20] Thus, in two-or one-photon excitation, $C_6^-$ is formed in the highly ro-vibrationally excited state in the ground electronic state,[21] which is the same as TNI formed in electron attachment. Recurrent fluorescence (RF) is a process of inverse internal conversion followed by an emission of a photon from the excited electronic state. RF has been recently detected in $C_6^-$.[22] Earlier, we have measured the absolute vibrational autodetachment (VAD), RF, and infrared (IR) cooling rates.[23] Owing to the high rate of RF processes, a TNI can effectively be stabilized against autodetachment by emitting a visible photon. By measuring rate coefficients for various competing decay channels of TNI, we have obtained an experimental estimate for the rate coefficient for the formation of stable $C_6^-$ anions by REA.

## II. EXPERIMENT

A schematic view of the experimental setup used to determine the decay rate coefficients of various competing processes such as vibrational autodetachment ($k_{VAD}(E)$), infrared cooling ($k_{IR}(E)$), and recurrent fluorescence ($k_{RF}(E)$) is shown in Fig. 2. Hot carbon cluster anions were produced in a Cs sputter source using graphite as a target. The ion beams were extracted and accelerated to 4.2 keV. A chopper produces ion bunches that are then mass selected by a 90° magnet and injected into a bent electrostatic ion beam trap (EIBT). The

[a]Electronic mail: vijayanand.chandrasekaran@weizmann.ac.il

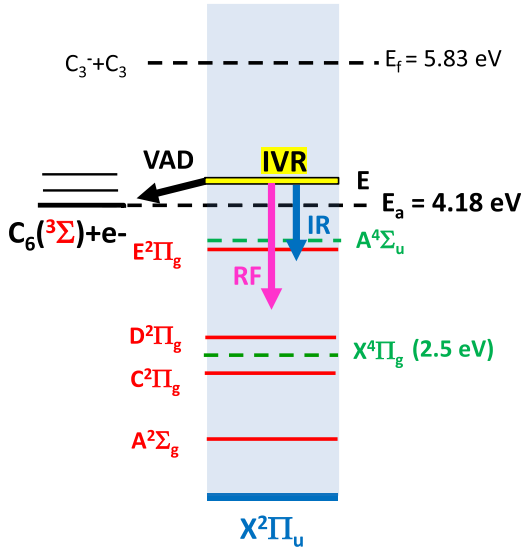


FIG. 1. Schematic representation of electron attachment processes to neutral $C_6$ leading to the formation of TNI in doublet and quartet excited $C_6^-$ anions. Various competing processes such as vibrational autodetachment (VAD) and radiative stabilization (infrared cooling and recurrent fluorescence cooling) are shown.

trap, which has been described in detail in Ref. 24, contains an electrostatic deflector that allows storage of the injected ions between two electrostatic mirrors in a V-shaped trajectory. About $10^4$–$10^5$ $C_6^-$ ions were injected into the trap by lowering the voltages of the entrance mirror electrodes for a time slightly shorter than their oscillation time $T_{osc} = 13\,\mu$s. The lifetime of the ions in the trap depends on the residual gas density. In the present experiment, the average lifetime of the ions is about 1 s. During this storage time, the ions are known to cool down vibrationally to approximately 350 K.[23]

At a given storage time $t_s$, ions located between the entrance mirror and the deflector were overlapped with a 5 ns-wide laser pulse with a pulse energy of $\lesssim$0.5 mJ, which was produced by an optical parametric oscillator pumped by a YAG laser. Both UV and visible photons were used to induce one- and two-photon excitations, respectively, of the $C_6^-$ anions to energies above the adiabatic detachment energy of 4.18 eV. While prompt decay products leave the trap undetected, neutral products resulting from decays that occur while the excited ions are traveling from the deflector towards the exit mirror can be detected in a microchannel plate detector (MCP) located behind the exit mirror. Thus the experiment is sensitive only to delayed neutralization processes. The shortest decay time contributing to the detected signal is determined by the transient time of the ions through the deflector and is estimated to be about 0.4 $\mu$s.

## III. RESULTS AND DISCUSSION

Typical delayed neutrals observed after the two-photon excitation of stored $C_6^-$ ions with a laser pulse at 606.9 nm are shown as a function of the delay time $t$ in Fig. 3. The spectrum was summed over $3 \times 10^3$ injections and corrected for neutrals resulting from the interaction of the stored (mainly unexcited) $C_6^-$ anions with the residual gas. Their contribution to the measured yield was determined from the number of neutralization events detected before the laser pulse. The delay time, $t$, was deduced from the measured time difference between the laser pulse and the arrival time of the neutral products at the MCP by subtracting a constant time interval reflecting the time-of-flight of the neutral products from the deflector to the MCP plus electronic delays. The spectrum obtained by binning the delay time into 1 $\mu$s bins is shown by the black dots in Fig. 3. The sawtooth-like peaks with a width of $\approx$6.5 $\mu$s clearly display the oscillation of the excited ions in the trap. Events observed between the peaks are due to the decay of $C_6^-$ ions while being slowed down in the exit mirror. By rebinning the spectrum using a bin size equal to the oscillation time $T_{osc} = 13.0\,\mu$s and plotting the results at times $t_i$ given by

$$t_i = iT_{osc} + 3.25\,\mu\text{s} \quad \text{with } i \geq 0 \tag{1}$$

(red squares in Fig. 3), most of these slowed down events are taken into account; simulations show that only a few percent of these events spill over to the next time bin. These rebinned decay curves, $R(t)$, are used for further analysis.

The delayed neutrals observed by the MCP after laser excitation of $C_6^-$ anions are solely due to the detection of the electron detachment products $C_6$. In principle, the detector is also sensitive to neutral fragmentation products such as $C_3$ resulting from the $C_6^-$ fragmentation channel with the lowest threshold energy of 5.83 eV. However already at excitation energies $E \approx 5.2$ eV, the decay rate due to VAD process is faster than $10^7$ s$^{-1}$ (see Fig. 4), i.e., the decay of these highly excited anions is expected to be "prompt." Moreover, the observed detachment products are solely due to the laser excitation of the doublet manifold. At laser wavelengths used in the present

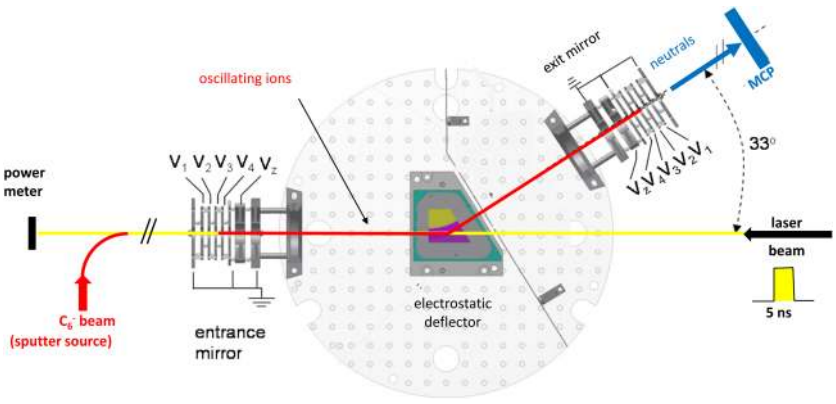


FIG. 2. Schematic view of the experimental setup, which employs a bent electrostatic ion beam trap.[24]

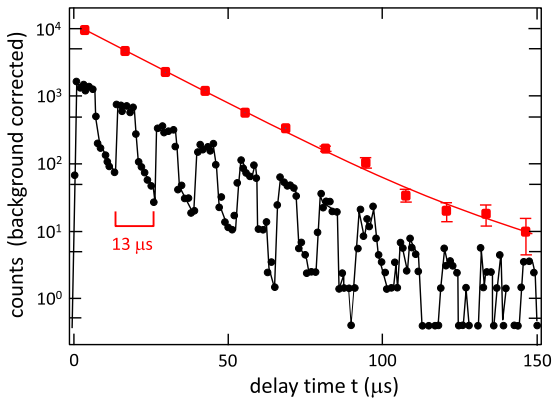


FIG. 3. Number of neutrals observed as a function of time after a two-photon excitation of $C_6^-$ with a 5 ns-wide laser pulse at a wavelength of 606.9 nm, summed over $3 \times 10^3$ injections and corrected for contributions caused by neutralization collisions of the stored $C_6^-$ ions with the residual gas. The laser pulse was fired 1 s after injection of the ions into the trap. (Black dots: 1 $\mu$s binning; red squares: binning to one oscillation period of 13.0 $\mu$s. Solid curves are a guide to the eye.)

investigation, the excitation of states with quartet symmetry—the lowest one being built on the $X^4\Pi_g$ state at $E = 2.5$ eV—leads to very fast decaying states with lifetimes outside the time window of our experiment. Finally, cascade decays of $C_6^-$ to states above $E_a$ can be neglected as the dominating RF decay involves transition energies >1 eV, leading directly to states below $E_a$. The observed laser-induced decay curves $R(t_i)$ within our detection window $r_\lambda(E,t)$ are thus given by

$$R(t_i) = N \int_{t_i-3.25\,\mu s}^{t_i+3.25\,\mu s} r(t)dt, \tag{2}$$

with

$$r(t) = \int_{E_a}^{\infty} r_\lambda(E,t)dE \tag{3}$$

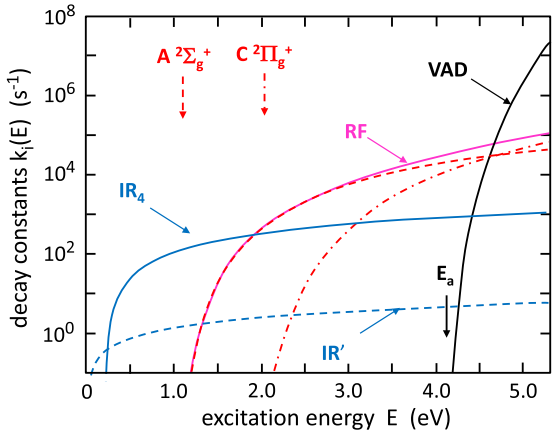


FIG. 4. Decay rate coefficients for various competing processes in $C_6^-$ using the PST relations derived in Sec. III A together with correction factors $f_{VAD} = 0.033$, $f_{RF} = 1.60$, $f_{IR,4} = 2.5$ determined in the present experiment (VAD: vibrational autodetachment; RF: recurrent fluorescence; $IR_4$: infrared transitions resulting from the asymmetric stretch mode; IR': infrared transitions involving all other active modes). The two partial RF decay coefficients mediated by the excited electronic configurations $A^2\Sigma_g^+$ and $C^2\Pi_g^+$ are shown by the dashed and dotted-dashed curves, respectively.

and

$$r_\lambda(E,t) = F_s(E = E_i + n_\lambda E_\lambda) \times k_{VAD}(E) e^{-k_{\rm tot}(E)t}. \tag{4}$$

Here $k_{tot}(E) = k_{VAD}(E) + k_{RF}(E) + k_{IR}(E)$ is the total decay constant, and $F_s(E_i)$ denotes the (normalized) vibrational energy distribution of $C_6^-$ after $t_s$ seconds of storage, which is shifted by the absorption of $n_\lambda$ photons of energy $E_\lambda$ from the laser pulse fired at time $t_s$. The integration is over all excitation energies greater than $E_a$ and $N$ is a normalization factor. Note that in writing Eqs. (3) and (4), it was assumed that the photon absorption cross section is constant over the width of $F_s(E_i)$.

Besides the delay-time dependence of $R(t_i)$, we will also analyze the total number of delayed neutralization events $\mathcal{R} = \sum_{t_0}^{t_f} R(t_i)$. When normalized to the number of photons per laser pulse (available from the measured laser pulse energy) and the number of stored ions at the time of the laser pulse (proportional to the number of residual gas-induced decays just before the laser pulse), the photon energy and storage-time dependence of $\mathcal{R}$ carry valuable information about $F_s(E_i)$.

### A. Decay of $C_6^-$ within phase space theory

Following Ref. 6, we use statistical PST to estimate the rate coefficients for vibrational autodetachment ($k_{VAD}(E)$), infrared radiative ($k_{IR}(E)$), and recurrent fluorescence ($k_{RF}(E)$). As shown in Fig. 1, the known electronic states of the $C_6^-$ ions below $E_a$ have either doublet or quartet symmetry, which are both accessible by attaching an electron to the $^3\Sigma_g$ ground state of $C_6$. For the time being, we shall only discuss the doublet manifold; the resulting formulas for the rate coefficients can be easily adjusted to deal also with the quartet states.

As discussed in some detail in Ref. 25, the delayed emission of an electron from an excited cluster, assumed to be subject to complete statistical mixing, can be related to the inverse process of electron capture by detailed balance, which is based on the equality of the forward and backward transition rates between two nondegenerate quantum states. Within this approach, the emission rate $k_{VAD}(E,\epsilon)$ of an electron with kinetic energy $\epsilon$ from a $C_6^-$ anion with total internal energy $E$ can be given by

$$k_{VAD}(E,\epsilon) = \frac{2\mu}{\pi^2\hbar^3}\sigma_c(\epsilon)\,\epsilon\,\frac{\rho(E - E_a - \epsilon)}{\rho_-(E)}. \tag{5}$$

Here, $\mu$ is the reduced mass of the electron, the factor of two accounts for the spin degeneracy of the emitted electron, $\sigma_c(\epsilon)$ is the electron capture cross section, and $\rho(E')$ and $\rho_-(E)$ denote the level densities of $C_6$ and $C_6^-$, respectively ($E' = E - E_a - \epsilon$ denotes the total energy of the neutral $C_6$ formed after photodetachment). In principle, the decay rates will depend on the total angular momenta $J'$ of $C_6$ and $J$ of $C_6^-$, which are dominated by the respective rotational angular momenta. Since the emission of an electron is not expected to change the rotational angular momenta, and the moment of inertias of the anion and the neutral cluster are very similar such that the rotational energies carried by $C_6$ and $C_6^-$ can be

assumed to be equal, we can ignore the rotational degree of freedom and consider the total energies $E'$ and $E$ to be carried only by the vibrational and electronic degrees of freedom (see also Ref. 25).

For lack of experimental data, the capture cross section $\sigma_c(\epsilon)$ has to be taken from theory. Instead of considering only $s$-wave electrons and approximating the capture cross section by its unitary limit, which was the approach taken by Terzieva and Herbst,[6] we will use the cross section derived by Voigt and Wannier (VW) (see, e.g., Ref. 26), allowing also for other than $s$-wave capture,

$$\sigma_c(\epsilon) = \frac{\pi\hbar^2}{2\mu\epsilon}\sum_l (2l+1)T_l(\kappa(\epsilon)). \tag{6}$$

Here $l$ denotes the angular momentum of the electron, and the function $T_l(\kappa(\epsilon))$ describes the probability for the capture of an $l$-wave electron in the polarization potential induced by the electron in $C_6$. $T_l(\kappa(\epsilon))$ is written as a function of the dimensionless parameter $\kappa$ given by

$$\kappa(\epsilon) = \mu\left(2\alpha e^2\epsilon\right)^{1/2}/\hbar^2, \tag{7}$$

where $e$ is the electron charge and $\alpha$ denotes the polarizability of $C_6$ ($\alpha = 15\times10^{-3}$ nm$^3$).[27] Analytical expressions for $T_l(\kappa)$ can be found in Ref. 26. In many applications of Eq. (5), the capture cross section is taken to be the classical Langevin cross section

$$\sigma_c(\epsilon) = \pi\left(\frac{2\alpha e^2}{\epsilon}\right)^{\frac{1}{2}}, \tag{8}$$

which is a very good approximation of Eq. (6) at electron energies higher than several tens of meV.

The level densities $\rho$ and $\rho_-$ are dominated by the vibrational level densities built on the electronic ground states $^3\Sigma_g$ and $^2\Pi_u$ of $C_6$ and $C_6^-$, respectively. In the absence of more advanced information, we will use the harmonic oscillator approach together with the counting method of Ref. 28 to calculate $\rho$ and $\rho_-$, using the respective (scaled) $s = 13$ fundamental vibrational frequencies, $\nu_s$, calculated in Refs. 29 and 30 for the two clusters in their electronic ground state configuration. While the approach is well justified for $C_6$, where the level density at low excitation energies is of interest, at excitation energies around $E_a = 4.18$ eV relevant for $C_6^-$, anharmonicities are expected to become important. In fact, schematic estimates using a Morse potential indicate that $\rho_-(E_a)$ can well be larger, by up to a factor of 10, than the harmonic oscillator value. By using the harmonic oscillator approach for $\rho_-$ in Eq. (5), we therefore expect to overestimate the VAD decay rate; to account for this and possible other shortcomings of our approach, we multiply the right hand side of Eq. (5) by a correction factor $f_{VAD}$, to be determined by experiment. The total vibrational autodetachment rate $k_{VAD}(E)$ for $C_6^-$ is thus approximated by

$$k_{VAD}(E) = \int_0^{E-E_a} \frac{2\mu}{\pi^2\hbar^3}\sigma_c(\epsilon)\,\epsilon \;\times f_{VAD}\, G\, \frac{\rho(E-E_a-\epsilon)}{\rho_-(E)}\, d\epsilon, \tag{9}$$

where $\rho$ and $\rho_-$ are the vibrational level densities built on the electronic ground state $^3\Sigma_g$ and $^2\Pi_u$ of $C_6$ and $C_6^-$, respectively, and $G$ denotes the ratio of the corresponding electronic degrees of freedom ($G = 3/2$).

It is straightforward to include also VAD decays to excited electronic states of $C_6$, such as the two lowest excited (singlet) states at 0.166 eV and 0.266 eV,[19] by modifying Eq. (5) accordingly. However, despite the rather low excitation energies, these contributions to the total VAD decay rate coefficient are expected to be at most a few percent in the relevant energy region, far below the accuracy we will achieve in our measurements; these contributions are therefore ignored.

Radiative cooling of the excited $C_6^-$ can take place via two processes: intra-electronic transitions between vibrational states built on the individual doublet states, which results in the emission of IR photons, and by inter-electronic transitions (RF) resulting in the emission of optical photons. To calculate the corresponding rate coefficients $k_{IR}(E)$ and $k_{RF}(E)$ within PST, we shall use again the harmonic oscillator frequencies to approximate the vibrational level density $\rho_-(E)$.

For estimating $k_{IR}(E)$, we even go a step further and apply the harmonic oscillator selection rules to estimate the IR transition rates. Ergo, we neglect overtone and interband IR transitions and only consider intraband transitions involving a change of the vibrational quantum number $n$ by −1, with Einstein coefficients given by $\mathcal{A}_s(h\nu_s)_{n\to n-1} = n\mathcal{A}_s(h\nu_s)$ in terms of the Einstein coefficient $\mathcal{A}_s(h\nu_s)$ describing the fundamental transition $1 \to 0$. In this approach, the IR decay rate coefficient is given by

$$k_{IR}(E) = \sum_s \mathcal{A}_s(h\nu_s)\sum_{n\geq 1} nP_{s,n}, \tag{10}$$

where $P_{s,n} = (\rho_-(E-nh\nu_s) - \rho_-(E-(n+1)h\nu_s))/\rho_-(E)$ denotes the probability of $C_6^-$ to be in a state that carries $n$ vibrational quanta $h\nu_s$. Inserting $P_{s,n}$ into Eq. (10), one obtains

$$k_{IR}(E) = \sum_s \mathcal{A}_s(h\nu_s)\sum_{n\geq 1}\frac{\rho_-(E-nh\nu_s)}{\rho_-(E)}. \tag{11}$$

In Eqs. (10) and (11), we neglected IR transitions occurring within vibrational bands built on excited electronic states with band head energies $E_j$, which is justified because $\rho_{j,-}(E) << \rho_-(E)$. The Einstein coefficients $\mathcal{A}_s(h\nu_s)$ for $C_6^-$ have been calculated from the infrared intensity from Ref. 29. The dominant IR transition is due to the asymmetric stretch mode ($s=4$) with $h\nu_4 = 0.23$ eV and $\mathcal{A}_4^{th} = 315$ s$^{-1}$, while for the other IR active transitions $\mathcal{A}_s^{th} < 1$ s$^{-1}$ ($\mathcal{A}_4^{th}$ and $\mathcal{A}_s^{th}$ indicate values from theoretical calculation). Since the latter are expected to influence the cooling process of $C_6^-$ only marginally within the time scale of our experiments, we will use the theoretical Einstein coefficients for estimating $k_{IR}(E)$ for all but the asymmetric stretch; for the latter we use $\mathcal{A}_4 = f_{IR,4}\mathcal{A}_4^{th}$, with a correction factor $f_{IR,4}$ to be determined by experiment.

Within PST, the partial recurrent fluorescence rate coefficients $k_{RF,j}(E)$ are given by

$$k_{RF,j}(E) = A_j(E_j)\frac{\rho_{j,-}(E)}{\rho_-(E)}, \tag{12}$$

where $A_j(E_j)$ denotes the Einstein coefficients for the transitions from the excited electronic state $j$ to the $X^2\Pi$ ground state

of $C_6^-$; based on level density arguments, energetically allowed transitions to excited electronic states can be neglected. As discussed already in Ref. 23, the RF process in $C_6^-$ is mediated by transitions from the $A^2\Sigma_g(j=1)$ state ($A_1^{th}(1.16\,\text{eV}) = 3.8\times10^5\ \text{s}^{-1}$)[31] and from the $C^2\Pi_g(j=2)$ level ($A_2^{th}(2.04\,\text{eV}) = 6.7\times10^6\ \text{s}^{-1}$),[32] while transitions from the higher lying $^2\Pi$ states are suppressed by their smaller $A_j$ values and their small statistical probabilities $P_j = \rho_{j,-}(E)/\rho_-(E)$ to be excited at excitation energies $E \lesssim E_a$. Approximating $\rho_{j,-}(E)$ by $\rho_-(E-E_j)$, the total decay rate coefficient $k_{RF}(E)$ can be written as

$$k_{RF}(E) = f_{RF}\sum_{j=1,2} A_j^{th}(E_j)\frac{\rho_-(E-E_j)}{\rho_-(E)}, \qquad (13)$$

where we introduced an overall correction factor $f_{RF}$ to be determined by experiment.

While the empirical correction factors introduced in the calculation of $k_{IR}(E)$ and $k_{RF}(E)$ will also take care of some of the assumptions and approximations made in the derivation of Eqs. (11) and (13), it should be kept in mind that the applicability of the phase space theory hinges on the level density being large enough to ensure a statistical equilibrium between the various degrees of freedom. In view of the fast electronic relaxation observed by Bragg *et al.*,[19] complete statistical mixing seems to take place already at excitation energies as small as ~1 eV, but might become questionable for energies below 0.4 eV, where the level density drops below 100 per $\text{cm}^{-1}$, sometimes considered to be the minimum density for this assumption to be valid.[33]

Decay-rate coefficients calculated for $C_6^-$ are displayed in Fig. 4 using correction factors determined in the experiments discussed in Secs. III B and III C.

### B. Determination of $k_{VAD}(E)$ and $k_{RF}(E)$

The decay rates $R(t)$ measured after laser excitation of $C_6^-$ exhibit close to exponential behavior over tens of microseconds (see, e.g., Fig. 6), which indicates that the average energy of the excited states contributing to $R(t)$ within this time span must be rather constant. Indeed, the integrand $r_\lambda(E,t)$ of the integral of Eq. (3), being limited on the high energy side by the strongly increasing total decay constant $k_{tot}(E)$ and on the low energy side by the steeply decreasing $k_{VAD}(E)$, is not only found to be strongly peaked around an average energy $\hat{E}_\lambda(t)$ defined by

$$\hat{E}_\lambda(t) = \int_{E_a}^{\infty} E\, r_\lambda(E,t)dE \Big/ \int_{E_a}^{\infty} r_\lambda(E,t)dE, \qquad (14)$$

but also to exhibit only a weak time dependence (see Fig. 5). We make use of the resultant close-to-exponential time dependence of $R(t)$ by fitting the measured decay rate for $t_i \geq t_0$ by

$$R(t) \propto e^{-k_\lambda t} \qquad (15)$$

and by interpreting $k_\lambda$ as the total decay constant at $E = \hat{E}_\lambda(t_0)$, i.e., $k_\lambda = k_{tot}(\hat{E}_\lambda(t_0))$. Moreover, due to the weak time dependence of the "observation window," $r_\lambda(E,t)$, and its narrow energy width, the delay-time integrated rate, $\mathcal{R}$, is a good measure of the population of states of the internal energy

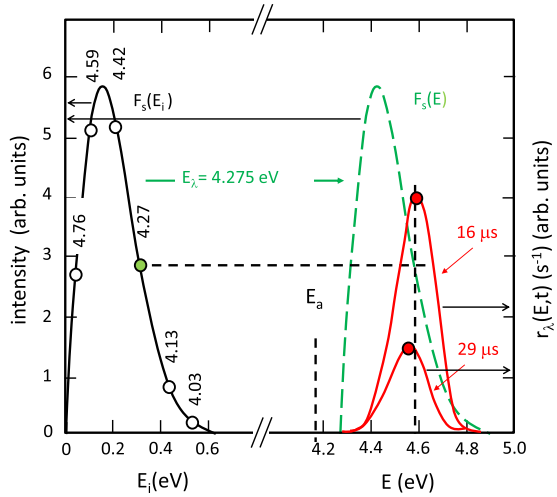


FIG. 5. Vibrational energy distribution $F_s(E_i)$ of $C_6^-$ before (black solid curve) and after absorption of a photon of energy 4.275 eV (green dashed curve), approximating $F_s(E_i)$ by a Boltzmann distribution for $T = 450$ K. The red solid curves are the integrands of $R(t)$, i.e., $r_\lambda(E,t)$, at a delay time of 16 $\mu$s and at 29 $\mu$s, covering a time span where the intensity of the integrand dropped by $1/e$, while the red dots denote the corresponding average energies $\hat{E}_\lambda(t)$. The open dots indicate the average internal energy at which the intensity of $F_s(E_i)$ is tested when absorbing a photon of an energy as given (in eV).

distribution $F_s(E_i)$ around $\langle E_i\rangle = \hat{E}_\lambda(t_0) - n_\lambda E_\lambda$ at the moment the laser is fired.

In our previous experiment[23] on $C_6^-$, we made use of this close-to-exponential behavior of $R(t)$ to determine the absolute scale of $k_{VAD}(E)$ and $k_{RF}(E)$ by deducing the corresponding correction factors $f_{VAD}$ and $f_{RF}$, respectively, using an iterative procedure. Decay curves were measured by exciting the anions after 1 s of storage by one- and two-photon absorption at different photon energies and fitted using Eq. (15) for $t_0 = 16.3\ \mu$s. The fitted decay constants $k_\lambda$ were first plotted as a function of $E = \hat{E}_\lambda(t_0)$ using $\hat{E}_\lambda(t_0)$ values calculated with first-guess correction factors, then $f_{VAD}$ and $f_{RF}$ were adjusted such that the calculated $k_{tot}(E)$ best represented the fitted values, and so on. Note that in the relevant energy region the contribution of $k_{IR}(E)$ to $k_{tot}(E)$ is very small (see Fig. 4); $f_{IR}$ was therefore fixed to the default value. The procedure resulted in $f_{VAD} = 0.030$ and $f_{RF} = 1.67$. The analysis was done by assuming $F_s(E_i)$ to be given by a bell-shaped distribution centered around ≈0.2 eV and a width of ≈0.2 eV, and although the results turned out to be rather insensitive to this assumption within their error margins, we redid the measurement with the aim of getting a better handle on the vibrational energy distribution at the moment of the laser shot.

The new measurement was done by exciting the $C_6^-$ ions after $t_s = 190$ ms of storage by one photon absorption. Employing one-photon excitation at several photon energies, we can use the integrated detachment rate $\mathcal{R}(E_\lambda)$ to gain information about the internal energy distribution at the instant of the laser pulse (see Fig. 5). Moreover, for storage times up to ~200 ms, the ions are still expected to be hot enough such that the development of the internal energy distribution as a function of storage time can still be described by a cascade process to be discussed below, which is based on the energy dependence of the radiative decay rate constants predicted within the statistical phase space approach.

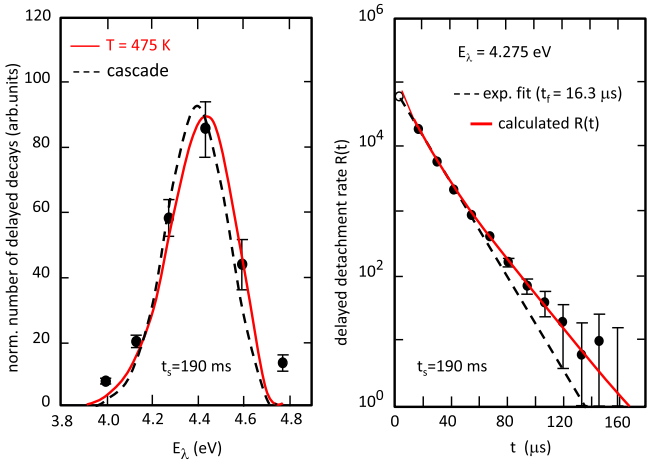


FIG. 6. Left panel: Normalized number of delayed decays $\mathcal{R}(E_\lambda)$ (16.3 $\mu$s $\leq t_i \leq$ 146.3 $\mu$s) after one-photon excitation of $C_6^-$ ions with a short laser pulse at several photon energies $E_\lambda$ (dots). The laser was fired 190 ms after injection of the anions into the trap. The solid curve is calculated assuming the internal energy distribution at the time of the laser pulse to be given by a Boltzmann distribution for a temperature $T$ = 475 K. The dashed curve is the result of a cascade calculation described in Sec. III C. Right panel: Detachment rate $R(t)$ observed at $E_\lambda$ = 4.275 eV as a function of the delay time $t$ (dots with statistical error bars). The dashed curve represents an exponential fit to the data, while the solid curve results from our statistical model calculation. The data corresponding to the first oscillation as indicated by the open circle have not been included in the analysis due to possible dead time effects of the MCP due to high event rate.

The observed number of delayed detachment events $\mathcal{R}(E_\lambda)$, summed over 16.3 $\mu$s $\leq t_i \leq$ 146.3 $\mu$s and normalized to the number of stored anions and to the number of photons in the laser pulses, is displayed as a function of the photon energy $E_\lambda$ in the left panel of Fig. 6. The solid line is the result of our statistical model calculation assuming that the internal vibrational energy distribution, $F_s(E_i)$, after 190 ms of storage is given by a Boltzmann distribution for a temperature of $T$ = 475 K. In view of the limited accuracy of the measured $\mathcal{R}(E_\lambda)$ values, caused mainly by uncertainties in the determination of the photon flux, and the simplifying assumption of a constant absorption cross section, the agreement is reasonable for temperatures $T$ = (475 ± 40) K.

The decay constants $k_\lambda$ deduced from fits to the measured decay curves $R(t)$ with Eq. (15) for decay times $t_i \geq t_0$ = 16.3 $\mu$s (an example is displayed in Fig. 6) are plotted in Fig. 7 as a function of $E = \hat{E}_\lambda(t_0)$; the energies $\hat{E}$ were calculated assuming a Boltzmann distribution for $T$ = 475 K and correction factors $f_{VAD}$ = 0.030 and $f_{RF}$ = 1.67. Since the Boltzmann distribution with its high energy tail seems to be the more realistic description of the vibrational energy distribution at long storage times than the symmetric Gaussian-like distribution used before (see also the discussion in Sec. III C), we also recalculated the $\hat{E}_\lambda(t_0)$ values deduced in Ref. 23 for the measurement at $t_s$ = 1 s using a Boltzmann distribution for $T$ = 350 K. Assuming $f_{IR,4}$ = 2.5, as estimated in Sec. III C, a global fit of the two sets of $k_{tot}(\hat{E}_\lambda(t_0))$ values, together with literature values for $k_{tot}(E)$ obtained at energies $E \gtrsim$ 5 eV by Zhao *et al.*,[21] with Eqs. (9), (11), and (13) results in

$$f_{VAD} = 0.033 \pm 0.005$$

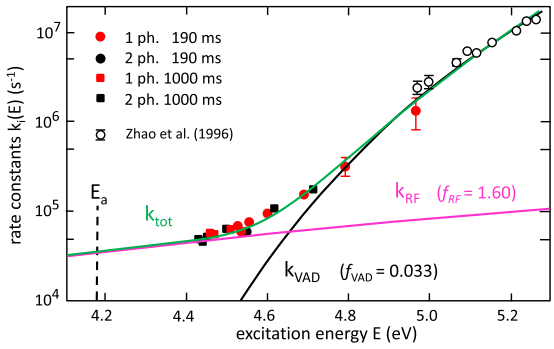


FIG. 7. Experimental decay-rate coefficients $k_\lambda$ deduced from exponential fits of the delayed detachment rates $R(t)$ for $t_0$ = 16.3 $\mu$s, plotted as a function of the total excitation energy $E = \hat{E}_\lambda(t_0)$ (symbols with statistical error bars). $\hat{E}_\lambda(t_0)$ is calculated assuming the internal energy distributions $F_s(E_i)$ at the time of the laser shot $t_s$ are given by a Boltzmann distribution for a temperature of $T$ = 475 K at $t_s$ = 190 ms and $T$ = 350 K at $t_s$ = 1000 ms. The solid green curve represents the sum $k_{tot}(E)$ of the partial decay rate coefficients for vibrational autodetachment, $k_{VAD}(E)$ (black curve), recurrent fluorescence $k_{RF}(E)$ (magenta curve), and infrared transitions $k_{IR}(E)$ (not shown) using Eqs. (9), (11), and (13) together with correction factors $f_{VAD}$ = 0.033, $f_{RF}$ = 1.60, and $f_{IR,4}$ = 2.5.

and

$$f_{RF} = 1.60 \pm 0.25.$$

No iteration was required as the old and new correction factors agree very well within their errors. For a final check of the accuracy of our results, the measured decay rates were compared to the calculated rates using Eq. (3), adjusting only the normalization. An example is shown in the right panel of Fig. 6; the data are indeed very well described.

The compatibility of an RF correction factor of $f_{RF}$ = 1.6 with the accuracy of the theoretical Einstein coefficients used in Eq. (13) has been discussed already by Chandrasekaran *et al.*[23] On the other hand, a large percentage of the correction factor $f_{VAD}$ needed to adjust $k_{VAD}(E)$ to the data has to be ascribed to the use of the harmonic level density for $C_6^-$ in Eq. (9), which leads to an overestimation of $k_{VAD}(E)$. In our previous work[23] and here, we have determined $k_{RF}(E)$ at energies higher than electron affinity. It is interesting to point out that recently the RF rates at lower excitation energies much below the electron affinity have been determined.[36]

### C. Determination of $k_{IR,4}(E)$

While the radiative cooling of $C_6^-$ around the adiabatic detachment energy is dominated by the RF process, the IR-active vibrational asymmetric stretch mode $s$ = 4 is expected to dominate the cooling process at excitation energies between ≈1.5 and ≈0.5 eV (see Fig. 4). As the $C_6^-$ anions leaving the sputter ion source are expected to be very hot, with internal energies much higher than 1.5 eV, and are known to reach average internal energies of ≈0.1 eV after 1 s of storage, the anions probe the relevant energy region while cooling down during storage in the trap. To follow the cooling down process, we used the integrated delayed detachment rates $\mathcal{R}(t_s)$ measured as a function of storage time $t_s$ while keeping the absorbed photon energy constant, similar to, approach followed in Refs. 37–39.

To describe the cooling of the hot $C_6^-$ ions leaving the sputter source, we use the master-equation approach.[35] In brief, discretizing the excitation energies $E$ of $C_6^-$ in bins of 16 meV and expressing the transition energies—assumed to be given by the fundamental transition energies—in multiples of this bin size, we follow the time development of the probability $P_i(t_s)$ that the $i$th energy bin is populated at time $t_s$ by solving the set of coupled differential equations $d\vec{P}(t_s)/dt_s = \mathcal{M}\vec{P}(t_s)$ with the initial condition $\vec{P}(t_s = 0)$. The matrix $\mathcal{M} = \{k_{i,j}\}$ is given by the rate coefficients for VAD, RF, and spontaneous and stimulated IR transitions. Using Eq. (9) with $f_{VAD} = 0.033$, Eq. (13) with $f_{RF} = 1.6$, and Eq. (11) with $\mathcal{A}_4 = f_{IR,4}\mathcal{A}_4^{th}$ and keeping $\mathcal{A}_s^{th}$ for all other IR transitions, we can calculate the internal energy distribution $F_s(E_i) \propto P_i(t_s)$ as a function of storage time with $f_{IR,4}$ being the only free parameter. The initial population $\vec{P}(t_s = 0)$ is assumed to be given by a Gaussian distribution around $E_a = 4.18$ eV, with a FWHM of 1 eV; however, the resulting internal energy distributions $F_s(E_i)$ for $t_s \gtrsim 5$ ms are independent of the detailed choice of $\vec{P}(t_s = 0)$, as long as the average initial energy is much larger than ≈1.5 eV: The radiative cooling mediated by the RF process is so fast that already 1 ms after their production the average excitation energy of the $C_6^-$ anions is down to ≈1.5 eV, where the cooling starts to be taken over by the considerably slower infrared transitions. The internal energy distribution $F_s(E_i)$, determined within this cascade model for a given storage time $t_s$, is then used to calculate the decay curve $R(t)$ and the time-integrated delayed detachment rates $\mathcal{R}(t_s)$.

$\mathcal{R}(t_s)$ observed after the absorption of two 606.9 nm photons ($2E_\lambda = 4.086$ eV) from the laser pulse by the $C_6^-$ ions are displayed in Fig. 8 as a function of the storage time $t_s$ at which the laser was fired. The rates were summed over delay time bins of $16.3\,\mu s \le t_i \le 94.3\,\mu s$ and were normalized to the number of ions stored at $t_s$ and to the square of the number of photons per laser pulse. The errors given (≈10%) are the estimated uncertainties caused by statistical fluctuations, but from the scatter of the $\mathcal{R}(t_s)$ values, it is obvious that the measurements are subject to much larger systematic errors that are likely caused by the limited stability and reproducibility of the laser alignment over several days of measuring time. Nevertheless, the data clearly show that the maximum of the laser-shifted internal energy distribution $F_s(E_i + 4.086\text{ eV})$ of the $C_6^-$ ions is passing over the detection window $r_\lambda(E, t)$ (see Fig. 5) while the ions are cooling down.

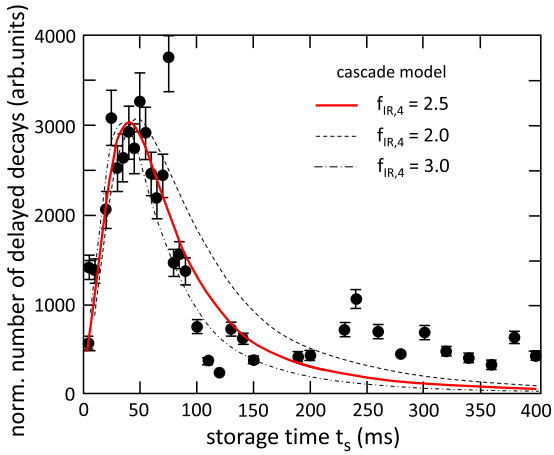


FIG. 8. Normalized time-integrated delayed detachment rates $\mathcal{R}(t_s)$ ($16.3\,\mu s \le t_i \le 94.3\,\mu s$), observed after two-photon excitation of $C_6^-$ ions with a short laser pulse of 606.9 nm photons, as a function of storage time $t_s$ (dots with error bars). The solid (dashed, dashed-dotted) curves are the results of our statistical model calculation changing the theoretical[29] Einstein coefficient $\mathcal{A}_4^{th}$ of the asymmetric stretch vibration by a factor $f_{IR,4} = 2.5$ (2.0, 3.0).

The curves plotted in Fig. 8 are the result of our cascade program when changing the adjustment factor $f_{IR,4}$ of $\mathcal{A}_4^{th}$. A reasonable representation of the maximum and the width of the measured $\mathcal{R}(t_s)$ distribution is obtained for

$$f_{IR,4} = 2.5\,^{0.5}_{0.3}.$$

Several remarks are in order when interpreting this result. The integrated delayed rates observed for storage times $t_s > 200$ ms are measuring the population of states with average energies between ≈0.4 eV and the threshold energy of 0.23 eV of the relevant infrared-active asymmetric stretch mode ($s = 4$), an energy region where the phase space theory is expected to fail, as discussed in Sec. III A. Indeed, while the measured $\mathcal{R}(t_s)$ values seem to stay almost constant for $t_s \gtrsim 200$ ms, the cascade calculation is obviously overestimating the radiative cooling of states below 0.4 eV. On the other hand, at shorter storage times where $\mathcal{R}(t_s)$ is mapping out the population and depopulation of states between 0.4 eV and 0.5 eV of the internal energy distribution $F_s(E_i)$, the cascade program still results in an acceptable description of the data given their large systematic uncertainties. This conclusion is collaborated by a comparison of the internal energy distribution $F_s(E_i)$ calculated within the cascade model for a storage time of $t_s = 190$ ms with the measured distribution displayed in Fig. 6 using $f_{IR,4} = 2.5$; indeed, a satisfying agreement between measured and calculated distribution is observed.

For storage times $t_s \le 40$ ms, the slope of $\mathcal{R}(t_s)$ also depends on the RF decay rate coefficient mediated by the excited electronic $A^2\Sigma_g^+$ state of $C_6^-$. The data, however, do not allow the determination of an individual correction factor for the assumed $A^2\Sigma_g^+$ to $X^2\Pi_u$ transition rate but corroborate the size of the global factor $f_{RF} = 1.6$.

The Einstein coefficient for the fundamental transition $1 \rightarrow 0$ of the asymmetric stretch vibration, needed to describe within the PST approach the IR-mediated radiative cooling of $C_6^-$, is thus found to be $\mathcal{A}_4 = 780\,^{160}_{100}\ s^{-1}$. Although a factor of 2.5 larger than the theoretical default value of 315 $s^{-1}$ used in the present study,[29] later theoretical calculations by the same authors[34] resulted in values of 360, 730, and 1600 $s^{-1}$. Our experimental estimate is well within the range of these theoretical predictions.

### D. Determination of rate coefficient for REA

With the absolute determination of the rate coefficients of all the competing processes of the TNI, namely, $k_{VAD}(E)$, $k_{RF}(E)$, and $k_{IR}(E)$, the rate coefficient for REA can be estimated. Considering for the time being only the population of the doublet manifold in $C_6^-$, the REA rate $\alpha(\epsilon)$ for an electron of energy $\epsilon$ to the electronic and vibrational ground state of $C_6$ is given within the present statistical treatment by

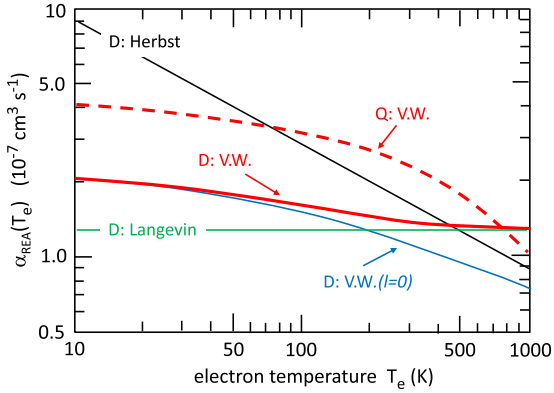


FIG. 9. Radiative electron attachment coefficients $\alpha_{REA}(T_e)$ for $C_6$ as a function of the electron temperature $T_e$. The solid and dashed red curves are the radiative electron attachment coefficients leading to doublet (D:V.W) and quartet (Q:V.W) manifold of $C_6^-$, respectively, using the capture cross section of Voigt and Wannier.[26] The thin curves are estimates of $\alpha_{REA}(T_e)$ by Ref. 6 (D:Herbst), and approximations using the Langevin cross section (D:Langevin) and assuming only s-wave scattering (D:V.W($l = 0$)).

$$\alpha_{REA}(\epsilon) = \frac{1}{2G}\sigma_c(\epsilon)\left(\frac{2\epsilon}{\mu}\right)^{1/2} b_{rad}(\epsilon), \tag{16}$$

where $b_{rad}(\epsilon)$ is the branching ratio describing the radiative stabilization of the highly excited $C_6^-$. The branching ratio, defined by

$$b_{rad}(\epsilon) = \frac{k_{RF}(E_a+\epsilon) + k_{IR}(E_a+\epsilon)}{k_{tot}(E_a+\epsilon)}, \tag{17}$$

is dominated for the doublet states by the RF process, leading to $b_{rad} > 0.99$ for $\epsilon \lesssim 300$ meV. While the branching ratio is well known from the present measurement, the use of the capture cross section in Eq. (16) is the most critical input. The product of the fraction of incomplete IVR and the fraction of vibrational excitation[40–42] has been represented by a correction factor $f_{VAD}$. On the other hand, attributing all of the $f_{VAD}$ to this quenching process may be unrealistic as well in view of the underestimated level density of $C_6^-$ when using harmonic vibrational frequencies. Thus Eq. (16) can provide at least an upper and lower limit to the radiative electron attachment rate by using the pure capture cross section or the one modified by $f_{VAD} = 0.033$.

To obtain the average radiative electron attachment coefficients for electrons of temperature $T_e$,$\alpha_{REA}(T_e)$, Eq. (16) is to be folded by a Maxwellian energy distribution. Results obtained assuming different unquenched capture cross sections are displayed in Fig. 9. For comparison, the attachment coefficient for quartet states are given as well, assuming doublet results for the correction factors as default values. Besides a factor of two, caused by the higher multiplicity of the quartet states, the main difference is due to the radiative stabilization, which leads to $b_{rad}(\epsilon) < 0.99$ for electron energies $\epsilon \gtrsim 10$ meV.

## IV. CONCLUSION

PST was used to describe the excitation energy dependence of the rate coefficients for vibrational autodetachment $k_{VAD}(E)$, recurrent fluorescence $k_{RF}(E)$, and infrared radiation due to the asymmetric stretch, $k_{IR,4}(E)$. Correction factors were introduced and adjusted to the experimental data to compensate for shortcomings of this approach, the use of theoretical transition probabilities and transition energies, and the usage of harmonic oscillator wave functions to estimate the level densities.

The impact of this approach on the accuracy of the extracted rate constants differs with excitation energy. For excitation energies $E_a \lesssim E \lesssim 4.7$ eV and for 4.6 eV $\lesssim E \lesssim 5.2$ eV, the contribution of these systematic errors to the uncertainties of the two rate coefficients $k_{RF}(E)$ and $k_{VAD}(E)$, respectively, and to the total rate coefficient $k_{tot}(E)$ is expected to be much smaller than their statistical errors of ±15%. On the other hand, for energies 0.5 eV $\lesssim E \lesssim$ 1.5 eV, where the asymmetric stretch is dominating the radiative cooling, $k_{IR,4}(E)$ is deduced rather indirectly from the development of the internal energy distribution with increasing storage times and the systematic errors are estimated to be of the size of the experimental error of ±20%. Unfortunately, in all three cases it is not possible to disentangle uniquely the different contributions leading to the deviations from unity of the correction factors $f_{VAD}$, $f_{RF}$, and $f_{IR,4}$: These factors can be reasonably well explained by level density arguments and/or the accuracy of the transition probabilities used.

By measuring the rate coefficient for all competing processes and using detailed balance as a link, the radiative electron attachment rate coefficient was estimated to be $3 \times 10^{-7}$ cm$^3$ s$^{-1}$ at 300 K, in agreement with the theoretical value of $1.7 \times 10^{-7}$ cm$^3$ s$^{-1}$. Such a high rate indicates that REA may play a prominent role in the formation of anions in the interstellar medium. Recurrent fluorescence was found to cool down the TNI. Our result clearly indicates that the anions can be formed in collision-less environments, such as interstellar medium, by radiative electron attachment.

## ACKNOWLEDGMENTS

This research was supported by the Israel Science Foundation (Grant No. 1242/09) and by the Benoziyo Endowment Fund for the Advancement of Science. We would like to acknowledge the key contribution to this paper by the late Professor Dirk Schwalm who passed away on July 14, 2016 while this work was in its final stages.

[1] C. M. McCarthy, C. A. Gottlieb, H. Gupta, and P. Thaddeus, Astrophys. J. **652**, L141 (2006).
[2] J. Cernicharo, M. Guélin, M. Agúndez, K. Kawaguchi, M. McCarthy, and P. Thaddeus, Astron. Astrophys. **467**, L37 (2007).
[3] P. Thaddeus, C. A. Gottlieb, H. Gupta, S. Brünken, M. C. McCarthy, M. Agúndez, M. Guélin, and J. Cernicharo, Astrophys. J. **677**, 1132 (2008).
[4] S. Brünken, H. Gupta, C. A. Gottlieb, M. C. McCarthy, and P. Thaddeus, Astrophys. J. **664**, L43 (2007).
[5] E. Herbst, Nature **289**, 656 (1981).
[6] T. Terzieva and E. Herbst, Int. J. Mass Spectrom. **201**, 135 (2000).
[7] S. Petrie and E. Herbst, Astrophys. J. **491**, 210 (1997).
[8] E. Herbst and Y. Osamura, Astrophys. J. **679**, 1670 (2008).
[9] N. Douguet, S. Fonseca dos Santos, M. Raoult, O. Dulieu, A. E. Orel, and V. Kokoouline, Phys. Rev. A **88**, 052710 (2013).
[10] N. Douguet, S. Fonseca dos Santos, M. Raoult, O. Dulieu, A. E. Orel, and V. Kokoouline, J. Chem. Phys. **142**, 234309 (2015).
[11] A. Canosa, D. C. Parent, D. Pasquerault, J. C. Gomet, S. Laubé, and B. R. Rowe, Chem. Phys. Lett. **228**, 26 (1994).

[12]R. L. Woodin, M. S. Foster, and J. L. Beauchamp, J. Chem. Phys. **72**, 4223 (1980).
[13]M. S. Foster and J. L. Beauchamp, Chem. Phys. Lett. **31**, 482 (1975).
[14]R. P. A. Bettens and E. Herbst, Astrophys. J. **478**, 585 (1997).
[15]T. J. Millar, Mon. Not. R. Astron. Soc. **259**, 35 (1992).
[16]C. Walsh, N. Harada, E. Herbst, and T. J. Millar, Astrophys. J. **700**, 752 (2009).
[17]T. J. Millar, C. Walsh, M. A. Cordiner, R. NíChuimín, and E. Herbst, Astrophys. J. **662**, L87 (2007).
[18]V. Wakelam, E. Herbst, J.-C. Loison, I. W. M. Smith, V. Chandrasekaran, B. Pavone, N. G. Adams, M.-C. Bacchus-Montabonel, A. Bergeat, K. Béroff, V. M. Bierbaum, M. Chabot, A. Dalgarno, E. F. van Dishoeck, A. Faure, W. D. Geppert, D. Gerlich, D. Galli, E. Hébrard, F. Hersant, K. M. Hickson, P. Honvault, S. J. Klippenstein, S. Le Picard, G. Nyman, P. Pernot, S. Schlemmer, F. Selsis, I. R. Sims, D. Talbi, J. Tennyson, J. Troe, R. Wester, and L. Wiesenfeld, Astrophys. J., Suppl. Ser. **199**, 21 (2012).
[19]A. E. Bragg, J. R. R. Verlet, A. Kammrath, and D. M. Neumark, J. Chem. Phys. **121**, 3515 (2004).
[20]C. Frischkorn, A. E. Bragg, A. V. Davis, R. Wester, and D. M. Neumark, J. Chem. Phys. **115**, 11185 (2001).
[21]Y. Zhao, E. de Beer, C. Xu, T. Taylor, and D. M. Neumark, J. Chem. Phys. **105**, 4905 (1996).
[22]Y. Ebara, T. Furukawa, J. Matsumoto, H. Tanuma, T. Azuma, H. Shiromaru, and K. Hansen, Phys. Rev. Lett. **117**, 133004 (2016).
[23]V. Chandrasekaran, B. Kafle, A. Prabhakaran, O. Heber, M. Rappaport, H. Rubinstein, D. Schwalm, Y. Toker, and D. Zajfman, J. Phys. Chem. Lett. **5**, 4078 (2014).
[24]O. Aviv, Y. Toker, M. Errit, K. G. Bhushan, H. B. Pedersen, M. L. Rappaport, O. Heber, D. Schwalm, and D. Zajfman, Rev. Sci. Instrum. **79**, 083110 (2008).
[25]J. U. Andersen, E. Bonderup, and K. Hansen, J. Phys. B: At., Mol. Opt. Phys. **35**, R1 (2002).
[26]E. I. Dashevskaya, I. Litvin, E. E. Nikitin, and J. Troe, Phys. Chem. Chem. Phys. **10**, 1270 (2008), Note that the analytical expressions for the l-wave capture probabilities given in the appendix have to be corrected for a printing error.
[27]O. Guliamov, L. Kronik, and J. M. L. Martin, J. Phys. Chem. A **111**, 2028 (2007).
[28]T. Beyer and D. F. Swinehart, Commun. ACM **16**, 379 (1973).
[29]J. Szczepanski, S. Ekern, and M. Vala, J. Phys. Chem. A **101**, 1841 (1997).
[30]J. Kurtz and L. Adamowicz, Astrophys. J. **370**, 784 (1991).
[31]Z. Cao and S. D. Peyerimhoff, J. Phys. Chem. A **105**, 627 (2001).
[32]X.-G. Gou, J.-L. Zhang, and Y. Zhao, J. Comput. Chem. **33**, 93 (2011).
[33]D. Boyall and K. L. Reid, Chem. Soc. Rev. **26**, 223 (1997).
[34]J. Szeczepanski, E. Auerbach, and M. Vala, J. Phys. Chem. A **101**, 9296 (1997).
[35]R. C. Dunbar and C. Lifshitz, J. Chem. Phys. **94**, 3542 (1991).
[36]N. Kono, T. Furukawa, H. Tanuma, J. Matsumoto, H. Shiromaru, T. Azuma, K. Najafian, M. S. Pettersson, B. Dynefors, and K. Hansen, Phys. Chem. Chem. Phys. **17**, 24732 (2015).
[37]M. Goto, A. E. K. Sundén, H. Shiromaru, J. Matsumoto, H. Tanuma, T. Azuma, and K. Hansen, J. Chem. Phys. **139**, 054306 (2013).
[38]K. Najafian, M. S. Pettersson, B. Dynefors, H. Shiromaru, J. Matsumoto, H. Tanuma, T. Furukawa, T. Azuma, and K. Hansen, J. Chem. Phys. **140**, 104311 (2014).
[39]G. Ito, T. Furukawa, H. Tanuma, J. Matsumoto, H. Shiromaru, T. Majima, M. Goto, T. Azuma, and K. Hansen, Phys. Rev. Lett. **112**, 183001 (2014).
[40]J. Troe, T. M. Miller, and A. A. Viggiano, J. Chem. Phys. **127**, 24403 (2007).
[41]J. Troe, T. M. Miller, and A. A. Viggiano, J. Chem. Phys. **130**, 244303 (2009).
[42]E. E. Nikitin and J. Troe, Mol. Phys. **110**, 1627 (2012).